Chemical Science

EDGE ARTICLE

View Article Online
View Journal | View Issue

Cite this: *Chem. Sci.*, 2016, **7**, 6988

Intrinsic high water/ion selectivity of graphene oxide lamellar membranes in concentration gradient-driven diffusion†

Pengzhan Sun,[ab] Renzhi Ma,*[b] Hui Deng,[a] Zhigong Song,[cd] Zhen Zhen,[ad] Kunlin Wang,[a] Takayoshi Sasaki,[b] Zhiping Xu*[cd] and Hongwei Zhu*[ad]

Received 29th June 2016
Accepted 16th July 2016

DOI: 10.1039/c6sc02865a

www.rsc.org/chemicalscience

Although graphene oxide lamellar membranes (GOLMs) are effective in blocking large organic molecules and nanoparticles for nanofiltration and ultrafiltration, water desalination with GOLM is challenging, with seriously controversial results. Here, a combined experimental and molecular dynamics simulation study shows that intrinsic high water/ion selectivity of GOLM was achieved in concentration gradient-driven diffusion, showing great promise in water desalination. However, in pressure-driven filtration the salt rejection was poor. This study unveils a long-overlooked reason behind the controversy in water desalination with GOLM and further provides a fundamental understanding on the in-depth mechanism concerning the strong correlation of water/ion selectivity with the applied pressure and GO nanochannel length. Our calculations and experiments show that the applied pressure weakened the water–ion interactions in GO nanochannels and reduced their permeation selectivity, while the length of nanochannels dominated the mass transport processes and the ion selectivity. The new insights presented here may open up new opportunities for the optimization of GOLMs in this challenging area.

Introduction

The graphene oxide (GO) lamellar membrane (GOLM), stacked from GO nanosheets with a unique sp^2 network spaced by various oxygen-containing functional groups, emerges as a rising star in filtration and separation due to its ultrafast water permeation with excellent selectivity toward the species dissolved.[1–10] Because of the steric hindrance of sp^2 nanocapillaries, large organic molecules and nanoparticles could be effectively sieved out for nanofiltration and ultrafiltration.[7,11–17] Meanwhile, due to the diverse electrostatic or chemical interactions between dissolved ions and active sites on the GOLM (*e.g.* sp^2 nanoclusters and oxygen functionalities),[5,6,9,10] excellent ion permeation selectivity could be achieved that may even afford water desalination considering the ultrafast water permeance.[1,2] Nanofiltration and ultrafiltration with GOLMs are generally accepted for removing solutes larger than the critical size of the nanocapillaries. However, water desalination with GOLMs is still very challenging and controversial results were reported: some showed that salt rejection of GOLMs and slightly reduced GOLMs was too poor for them to be promising in water desalination,[11–14,16] while others reported the opposite.[17–19] This controversy impedes further research and development of GOLMs toward practical desalination applications. Considering that water desalination with GOLMs is one of the most promising yet challenging developing directions with great implications in addressing the worldwide crisis of fresh water shortage and contamination, a consensus must be reached about whether GOLMs have desalination abilities and how to fully exploit their potential before the deployment of this newly emerging membrane material in this area.

In this study, through a combination of isotope labelling-assisted synchronous investigation of water and ion diffusion, pressure-driven filtration and molecular dynamics (MD) simulations, we show a great potential for GOLMs in water desalination because of their intrinsic high water/ion selectivity in concentration gradient-driven diffusion. However, their salt rejection (*i.e.* water/ion selectivity) was poor in pressure-driven filtration. This discrepancy was found to originate from the strong correlation of water/ion selectivity with the applied pressure and GO nanochannel length. The applied pressure weakened the water–ion interactions confined in GO nanochannels and further reduced their selectivity when permeating through, while the nanochannel length dominated the water

[a]*State Key Laboratory of New Ceramics and Fine Processing, School of Materials Science and Engineering, Tsinghua University, Beijing 100084, China. E-mail: hongweizhu@tsinghua.edu.cn*

[b]*International Center for Materials Nanoarchitectonics (WPI-MANA), National Institute for Materials Science (NIMS), 1-1 Namiki, Tsukuba, Ibaraki 305-0044, Japan. E-mail: MA.Renzhi@nims.go.jp*

[c]*Department of Engineering Mechanics, Tsinghua University, Beijing 100084, China. E-mail: xuzp@tsinghua.edu.cn*

[d]*Center for Nano and Micro Mechanics (CNMM), Tsinghua University, Beijing 100084, China*

† Electronic supplementary information (ESI) available: Materials and methods, supplementary text and figures. See DOI: 10.1039/c6sc02865a

and ion transport processes and regulated the selectivity among various salts (Fig. 1). The new insights presented here throw light upon the in-depth mechanism of water desalination with GOLMs and assist the future development of GOLMs in this promising yet challenging area.

Results and discussion

Concentration gradient-driven diffusion

A monolayer GO nanosheet aqueous suspension was vacuum-filtered through a microfilter (*e.g.* polyvinylidene fluoride (PVDF) filter paper or anodized aluminium oxide (AAO) disc) to prepare GOLMs. Characterizations of GO nanosheets and GOLMs with atomic force microscopy (AFM), X-ray diffraction (XRD) and scanning electron microscopy (SEM) are shown in Fig. S1†.[20] According to recent studies on the structure of GOLMs in various solvents and solutions,[21–23] the interlayer spacing of GOLMs remained stable in acidic and neutral aqueous solutions, which was close to or slightly higher than the value in pure water. However, the GOLMs would gradually disintegrate in some basic solutions with certain concentrations. Therefore, strong basic salt solutions were avoided in this study to ensure the structural stability of GOLMs and their interlayer distances in various aqueous solutions were assumed to be equivalent to the value in pure water (*i.e.* 1.32 nm, Fig. S1†). Note that membrane-based water desalination means the transmembrane transport rate of water is faster than that of dissolved ions (*i.e.* water/ion selectivity > 1). In order to quantify this with GOLMs, concentration gradient-driven diffusion experiments were first performed, as shown in Fig. 1 (top inset) and S2A and B†.[20]

The GOLMs used in the diffusion experiments were micron-thick (Fig. 1, bottom inset), consistent with most of the previous concentration gradient-driven mass transport studies,[1,3,5–8] in which thousands of GO layers were stacked into a lamellar structure. The leakage through the intrinsic defects of the GO flakes, which only occupied a tiny areal percentage,[8,24–26] could be effectively minimized due to mutual stacking. Therefore, mass transport should mostly occur through the sp^2 nano-capillaries in the GO interlayer galleries,[1,3,5–8] deviating from the cases of selective gas transport through few-layered GOLMs.[27,28]

In a typical concentration gradient-driven diffusion experiment, equivalent volumes of a certain salt solution and deionized water were injected into the feed and permeate reservoirs separated by a GOLM on a microfilter (PVDF). The GOLM was not detached from the microfilter because the microfilter could provide valuable mechanical support to improve the membrane stability in solutions. Control experiments were conducted with bare microfilters to subtract the effect of the porous support. Diffusivities (D) of water and salt through bare microfilter and GOLM were determined to reflect their intrinsic transmembrane permeation abilities (Fig. S3†).[20]

The salt permeation was extrapolated from the permeate conductivity variation with time. In order to detect water permeation, which was prevented by the absence of micro- or macroscopic differences between the feed and permeate water, an isotope labelling technique was utilized as follows: with deuterium oxide (D_2O), an isotope of H_2O, as a tracer to label the feed solution, the permeance of D_2O with time was measured with attenuated total reflection Fourier transformed infrared spectroscopy (ATR-FTIR); by quantifying the permeation differences between D_2O and H_2O (diffusivity ratio of H_2O/D_2O through GOLM was determined as ~1.4), water permeation was extrapolated (Fig. S4–S6†).[20] Using this isotope labelling technique, water and salt transmembrane diffusion could be synchronously investigated. As shown in Fig. 2A and B, both water and salt transmembrane permeations of representative KCl and $K_3Fe(CN)_6$ feed solutions were linear. Permeation rates of solvent water through bare microfilter were equivalent

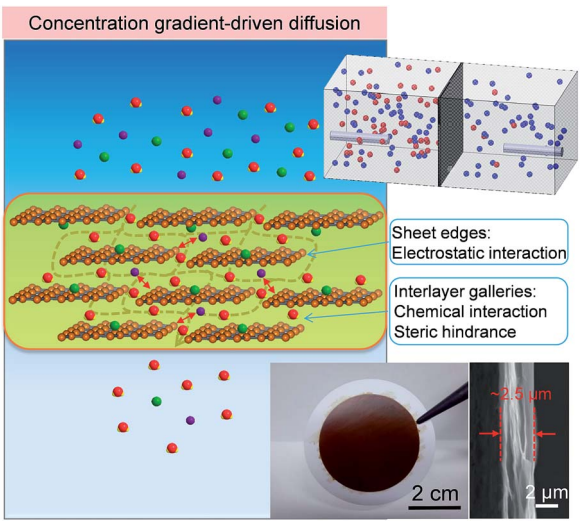

Fig. 1 Schematic for the mechanism of water desalination, experimental setup and photograph of GOLM on a microfilter with a cross-sectional SEM image for concentration gradient-driven diffusion.

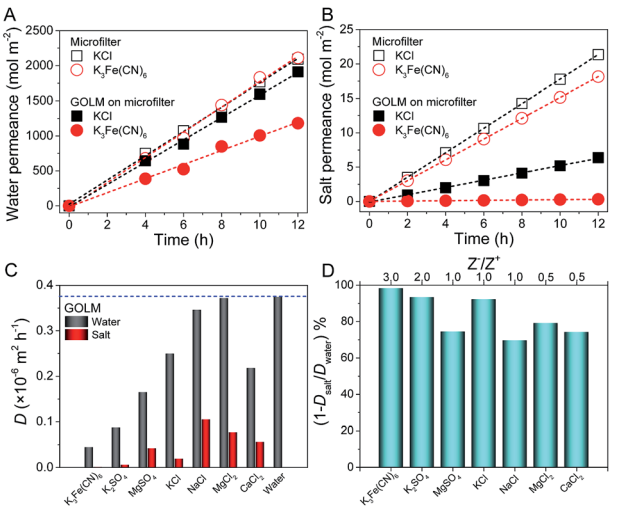

Fig. 2 Representative (A) water and (B) salt transmembrane permeations. Feed concentration of salts: 0.1 M; feed concentration of D_2O: 30 wt%. (C) Diffusivities of various salts and corresponding solvent water through GOLM. (D) Calculated nominal rejections for various salts through GOLM in diffusion.

(Fig. 2A), but the permeation rate of $K_3Fe(CN)_6$ salt was slightly lower than that of KCl (Fig. 2B) due to its larger size. Compared to bare microfilter, with ~2.5 μm-thick GOLM on the microfilter, the water permeations of KCl and $K_3Fe(CN)_6$ feed solutions were reduced by 8% and 44% (Fig. 2A), while the salt permeations were reduced by 70% and 98% (Fig. 2B), respectively. As shown in Fig. S7,† the permeate solutions corresponding to 0.1 M $K_3Fe(CN)_6$ feed solution through bare microfilter and GOLM on microfilter indicated an effective sieving of $K_3Fe(CN)_6$ by the GOLM. These results reveal that water could permeate through the GOLM rapidly except when partially blocked by large solutes (*e.g.* $K_3Fe(CN)_6$), while salts could be effectively captured or blocked by the GOLM, resulting in an excellent water/ion selectivity for possible desalination uses.

The transmembrane permeations of a wide range of salts and the corresponding solvent water were studied. Diffusivities through bare microfilter were calculated and are listed in Fig. S8.† After the effect of the microfilter was subtracted (Fig. S3†),[20] diffusivities through GOLM were calculated and are summarized in Fig. 2C. Generally, the diffusivities of solvent water through GOLM were about one order of magnitude lower than through microfilter, and those of salts were even lower. However, by considering their microstructures, the diffusivities of water and salts through the nanocapillaries in GOLM were estimated to be orders of magnitude greater than through the sub-micron-sized channels in PVDF microfilter (Fig. S9†).[20] With bare microfilter (Fig. S8†), various salts diffused through with insignificant selectivity and corresponding solvents diffused through with nearly the same rate as pure water. Permeations of various salts were slightly faster than water, indicating that the microfilter did not have desalination ability and its water/ion selectivity was <1. By contrast, with GOLM (Fig. 2C), diffusivities of solvent water were all significantly greater than salts, indicating effective desalination. Excellent selectivity in ion diffusion rates was achieved with GOLM (Fig. 2C) because of its steric hindrance from sp^2 nanocapillaries, and electrostatic and chemical interactions from the active sites on GOLM.[5,6,10,20] Notably, diffusions of solvent water were slower than pure water and different salts gave different water diffusivities, indicating that the ion–water interactions (*i.e.* ion hydration–dehydration effects) confined in GO nanochannels led to different degrees of blockage to the transport of water. According to the physical nature of membrane-based water desalination, a nominal rejection was defined as $R_n = 1 - D_{salt}/D_{water}$ to reflect the relative removal of salt ions with respect to water molecules in diffusion. As shown in Fig. 2D, a summary of the nominal rejections for studied salts, GOLM had excellent water desalination performance, with all the rejections >70%. In particular, because $K_3Fe(CN)_6$, K_2SO_4 and KCl were confronted with either effective steric hindrance from sp^2 nanocapillaries, strong electrostatic repulsion from ionized oxygen functionalities or cation–π capture from sp^2 aromatic clusters, their rejections were above 90%. These results indicate that by taking full advantage of the steric effect and diverse interactions originating from the unique structure and composition of GOLM, excellent salt rejection with high water permeance could be achieved, showing great potential in water desalination.

pH and ion concentration effects

As indicated in the XRD patterns (Fig. S1B†), the size of the void space in the GO interlayer galleries (*i.e.* sp^2 nanocapillaries) was ~0.97 nm in the fully wet state, which was responsible for mass transport in solutions.[20] This critical size was able to generate a sieving effect based on steric hindrance or hydrodynamic interaction with the nanocapillary walls for effective ion rejection, as for that of $K_3Fe(CN)_6$ (hydrated diameter of $Fe(CN)_6^{3-}$: 0.95 nm) in both processes. Additionally, the electrostatic or chemical interactions between ions and GO might also contribute to ion rejection. When the solution pH is increased, oxygen functionalities on GO (*e.g.* carboxyl groups) become deprotonated and negatively charged. Consequently, ion rejection can be increased owing to the enhancement of electrostatic repulsion toward anions. On the other hand, ion rejection should be highly sensitive to the degree of electrostatic screening, *i.e.* ion concentration, if electrostatic interaction plays a role.

To study the importance of electrostatic interaction, water and ion permeations and salt rejection were measured as a function of pH and ion concentration (Fig. 3).[20] Firstly, the diffusions of water and ions through GOLM were measured at three pH values with 0.1 M KCl feed solutions, as shown in Fig. 3A. The pH-dependent diffusivity variations of K^+ and Cl^- ions through GOLM were insignificant, suggesting that the electrostatic interaction did not play a major role in ion transport. On the other hand, the water diffusivity had a significant increase in both acidic (pH = 3.6) and basic (pH = 9.3) cases compared to the unadjusted case (pH = 5.9), indicating that the presence of extra H^+ or OH^- accelerated water transport,

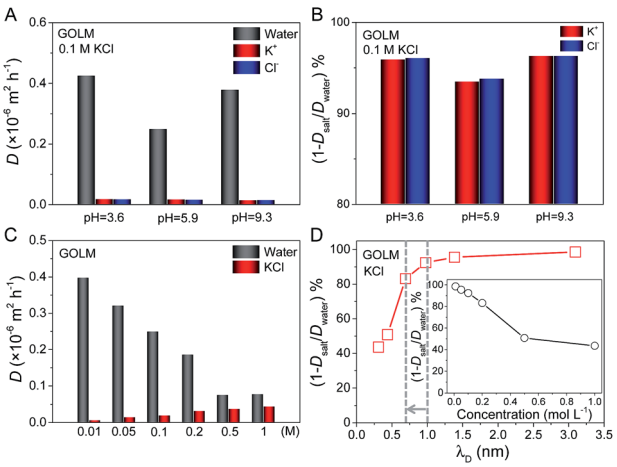

Fig. 3 (A) pH-dependent diffusivities of water and ions through GOLM for 0.1 M KCl feed solutions. (B) Corresponding nominal rejections of K^+ and Cl^- ions in diffusion. (C) Ion concentration-dependent diffusivities of water and KCl through GOLM. (D) Corresponding nominal KCl rejections as a function of Debye screening length (λ_D) in diffusion. The inset shows the dependence of nominal KCl rejections on ion concentration.

presumably originating from the effective promotion of water migration by the rapid H^+ and OH^- propagations through the hydrogen-bonding networks along the water layers formed in the GO interlayer galleries.[29] The corresponding nominal ion rejections were calculated and are shown in Fig. 3B, revealing that due to the enhancement of water transport, the ion rejections were enhanced in acidic and basic cases compared to the unadjusted case. Note that the ion rejections were all above 90% and the value at pH = 9.3 was only ~0.3% and ~2.8% higher than those at pH = 3.6 and 5.9, respectively, well below the expectation from electrostatic interaction, implying its negligible role in ion rejection with the micron-thick GOLM in diffusion. According to ref. 6, the cation–π interaction between K^+ and the sp^2 nanoclusters on GO was strong enough to induce an effective capture. Therefore, for the rejection of KCl with GOLM in diffusion, the cation–π interaction which occurred in sp^2 nanocapillaries would play a dominant role.

Next, taking KCl as an example, the concentration-dependent water and ion diffusion through GOLM was measured, as shown in Fig. 3C. The diffusivities of water and ions were sensitive to the variations in electrolyte concentration: the salt diffusivity increased while the water diffusivity decreased with increasing ion concentration, indicative of a strong competition between water and ion permeation. The nominal salt rejections are plotted as a function of Debye screening length (λ_D, $\lambda_D \propto c^{-1/2}$) in Fig. 3D, and their relationship with the electrolyte concentration is shown in the inset. Typically, for a charged capillary with a diameter greater than the permeated ions, a significant rejection of co-ions is expected when λ_D (reflecting the range of electrostatic interaction) is much larger than the diameter of the capillary. Due to the electroneutrality requirement, the counter-ions are also rejected. As λ_D becomes comparable to the dimension of the capillary, a rapid decrease in salt rejection is expected due to the quick decay of the electrostatic potential with $1/\lambda_D$. As indicated in Fig. 3D, the nominal salt rejection began to drop sharply at a λ_D of ~0.7 nm. However, this value was smaller than the critical size of sp^2 nanocapillaries in GOLM (~0.97 nm, Fig. S1B†). Notably, the rejection dropped more slowly afterwards; even when λ_D was decreased to ~0.3 nm, a rejection rate of >40% could still be preserved. These results again indicate that the electrostatic interaction was not the major cause of salt rejection in diffusion, in agreement with the pH-dependent measurements in Fig. 3A and B. The reduced rejections with increasing electrolyte concentration could be simply attributed to the variations in driving forces for water and salt transport: the increased ion concentration gradient promoted salt transport while the increased osmotic pressure prevented water transport.

Pressure-driven filtration

For comparison, pressure-driven filtration experiments were performed with GOLM (on AAO) in a dead-end filtration device pressurized with N_2 gas flow (top inset in Fig. 4 and S2C†).[20] In order to gain a relatively high water permeability, several hundred nanometer-thick GOLMs (Fig. 4, bottom inset) were used in pressurized filtration experiments, which were one order of magnitude thicker than the previous studies[11,12] to avoid leakage through large defects or discontinuity and to unveil the intrinsic pressurized mass transport properties. Because the AAO porous support contributed little to the flux and salt rejection of GOLM under pressure, control experiments with bare AAO discs were ignored. According to recent studies on the pressure-controlled separation performances of GOLMs,[15,30] the interlayer galleries within GOLMs were relatively stable at low pressures because of their rigidity. However, these nanochannels would collapse and shrink at high pressures. Therefore, in this study, a low pressure of 0.1 MPa was applied in order to minimize the pressure effect on the structural stability of GO interlayer nanochannels.

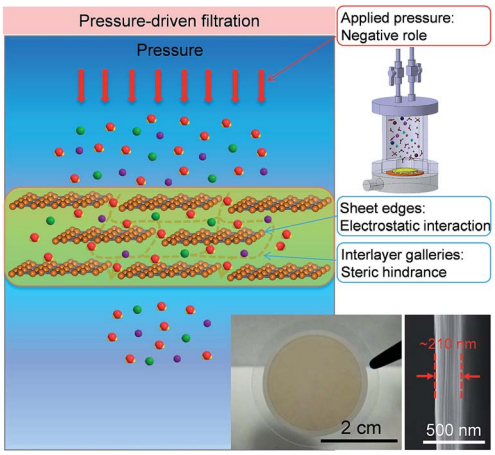

Fig. 4 Schematic for the mechanism of water desalination, experimental setup and photograph of GOLM on a microfilter with a cross-sectional SEM image for pressure-driven filtration.

Various feed solutions were allowed to percolate through the GOLM under a pressure of 0.1 MPa, and corresponding permeate solutions were collected over time to measure the flux and salt rejection. Fig. 5A shows the fluxes of pure water, 0.5 mM KCl and $K_3Fe(CN)_6$ feed solutions from at least three repeated experiments. The inset in Fig. 5A shows the representative time variations of permeate volumes per unit area, indicating that the permeate volumes increased nonlinearly with time. Plots collected after 1 h were fitted into linear relationships and the slopes were equivalent to the fluxes. As shown in Fig. 5A, the fluxes of salt solutions were lower than those of pure water, in agreement with the diffusion experiments (Fig. 2C). However, no significant differences in flux were detected for different salt solutions, contrary to the case for diffusion, indicating that the applied pressure would weaken the ion–water interactions and result in collective transport of water and ions through the GOLM with weaker mutual interaction.

As shown in Fig. 5B, rejections of GOLM toward a wide range of feed solutions in pressurized filtration were measured, which were highly sensitive to anion/cation valence ratios (Z^-/Z^+), indicating that the electrostatic interaction played a major role. Typically, negative charges on GO electrostatically repel anions and attract cations. The electroneutrality requirement of the

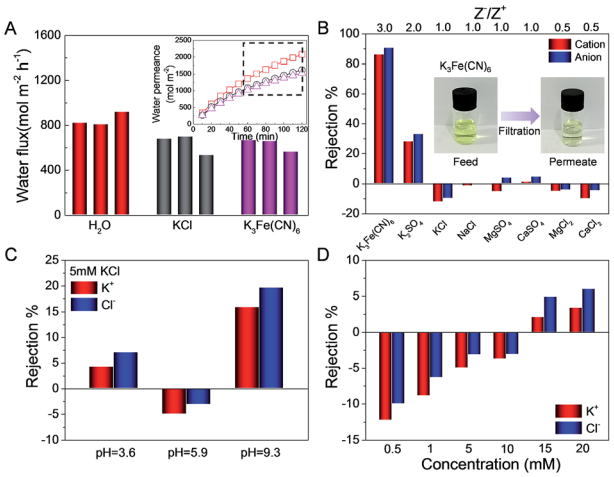

Fig. 5 (A) Fluxes through GOLM in pressurized filtration for various feed solutions. The inset shows the representative time variations of permeate volumes per unit area. Applied pressure: 0.1 MPa. (B) Rejections of various salts in pressurized filtration with GOLM. Feed concentration: 0.5 mM. The insets show photographs of $K_3Fe(CN)_6$ feed and permeate solutions. (C) pH-dependent K^+ and Cl^- rejections of GOLM toward 5 mM KCl feed solutions in pressurized filtration. (D) Ion concentration-dependent K^+ and Cl^- rejections of GOLM in pressurized filtration.

permeate solution prevents the independent migrations of cations and anions. Therefore, the salt rejection depends on the competition between opposite electrostatic forces, *i.e.* higher Z^-/Z^+ means stronger net repulsion and higher rejection. Indeed, the rejection dropped sharply with the decrease of Z^-/Z^+, approaching zero for salts with Z^-/Z^+ of ≤ 1. In particular, the rejection of $K_3Fe(CN)_6$ was the highest ($\sim$90%), due to the synergistic effect of strong steric hindrance and net electrostatic repulsion originating from its large dimension and high Z^-/Z^+. The insets in Fig. 5B of the $K_3Fe(CN)_6$ feed and permeate solutions reveal that most of the brown-colored species were removed, showing the potential of GOLM in pressure-driven specific large-ion desalination. Furthermore, salt rejections in pressurized filtration were all significantly lower than in diffusion, implying that the applied pressure would play a negative role in desalination with GOLM.

The pH-dependent ion rejections of GOLM in pressurized filtration were measured with 5 mM KCl feed solutions, as shown in Fig. 5C. The change in tendency of ion rejection as a function of pH was consistent with that in diffusion (Fig. 3B), confirming the role of extra H^+ and OH^- in accelerating water transport and further increasing the ion rejection. By contrast, the rejection was highly sensitive to pH variations, *e.g.* the value at pH = 9.3 was $\sim$2.1 times and $\sim$5.4 times higher than those at pH = 3.6 and 5.9, respectively, much greater than in the diffusion case, indicating that the electrostatic interaction played a significant role in pressurized filtration through the several hundred nanometer-thick GOLM.

The concentration-dependent salt rejections of GOLM in pressurized filtration were measured, as shown in Fig. 5D. Surprisingly, the rejection increased with the electrolyte concentration, deviating from the expected tendency as in diffusion. This discrepancy might be explained by the role of pressure in rejection: increasing the electrolyte concentration should enhance the resistance (*e.g.* osmotic pressure) against the direction of applied pressure, further gradually counteracting the pressure and weakening its negative effect on salt rejection. The pH- and ion concentration-dependent permeations and rejections of GOLM in diffusion and pressurized filtration were in stark contrast to the cases of carbon nanotube forests bearing aligned graphitic nanochannels with negatively charged groups at the entrances,[31] showing the unique mass transport properties of GOLM originating from its intrinsic lamellar structure and composition.

Molecular dynamics simulations

To interpret the discrepancy in the obtained experimental results and gain an atomistic insight into the role of pressure in the transport of water and ions through the nanochannels in GO interlayer galleries, MD simulations were performed.[20] The simulation results illustrated in the inset of Fig. 6A show that as nanoconfinement was applied, the mean residual time (MRT) of the first solvation shell around the ions was reduced, and the applied driven pressure further lowered the MRT for ions confined in GO nanochannels (Fig. 6A). Consequently, the effect of mass contrast between ion (with its solvation shell) and water molecule was reduced, resulting in the lowered water/ion selectivity in pressurized filtration compared to that in diffusion (Fig. 6B). With the increase of applied pressure gradient, the MRT of water molecules in the first solvation shell of ions between GO sheets was further reduced (Fig. 6A). The ion became less protected by the solvation shell and its interaction with the GO walls became more dominant, resulting in an increase of water/ion selectivity with the applied pressure gradient (Fig. 6B). However, in the whole range of pressure gradient studied, the water/ion selectivity was always lower than that in nanoconfined diffusion, confirming the negative role of pressure in water desalination with GOLM, consistent with the experimental results in Fig. 2D and 5B. It should be remarked here that due to the limitation of time span in the MD simulations, the pressure gradient applied in simulations was higher than the value in experiments. Nevertheless, the conclusions here still held qualitatively, if not quantitatively, and the experimental scale could be considered as the lower limit of the pressure gradient in the MD simulations.

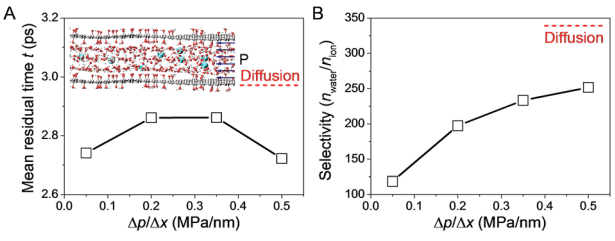

Fig. 6 (A) Mean residual time of water molecules in the first solvation shell of ions between GO sheets obtained from MD simulation. (B) Simulated water/ion selectivity of pressure-driven filtration, compared to ionic diffusion confined in GO nanochannels.

GO nanochannel length effects

To further explore the in-depth mechanism of water desalination with GOLM, we noted two major differences in diffusion and pressurized filtration, including driving force and GOLM thickness (*i.e.* GO nanochannel length), which might serve as the origin of the discrepancy in desalination. The experiments and calculations in Fig. 2, 5 and 6 have shown that the applied pressure caused a negative effect on water desalination. Here, effects of GOLM thickness were studied by monitoring its evolutional vacuum-assisted formation process and corresponding ion transmembrane permeations without considering the related water permeations.[20] As shown in Fig. S10,† the porous substrate was gradually covered with GO nanosheets followed by the emergence of wrinkles. Meanwhile, corresponding ion permeations shown in Fig. S11† indicate that significant selectivity in ion fluxes was observed with the formation of wrinkles, implying the presence of large defects or discontinuity with serious leakage in thinner GOLMs. Additionally, the tendency in ion selectivity exhibited a clear transition with the increase of GOLM thickness: electrostatic interaction was a major contributor to the ion selectivity of thinner GOLMs with more sheet edges (*i.e.* short GO nanochannels), while chemical interaction began to dominate in thicker GOLMs with more interlayer galleries (*i.e.* long GO nanochannels). In particular, the tendency in ion fluxes through a GOLM with the same thickness as that in pressurized filtration (Fig. S11E†) was just opposite to the tendency in pressurized rejections (Fig. 5B). This indicates that the nanochannel length-correlated ion selectivity contributed substantially to the salt rejection of GOLM, but the ion–water interaction was seriously weakened in pressurized filtration due to the independence of salt rejection on the transport of water, deviating from the diffusion case (Fig. 2D) and consistent with the MD simulations (Fig. 6).

The transmembrane water and salt diffusion fluxes through GOLMs with increased thickness were synchronously measured with $K_3Fe(CN)_6$, K_2SO_4 and KCl feed solutions (Fig. 7A and B). The results show that water flux through GOLM (on microfilter) was independent of the membrane thickness (*i.e.* the length of nanocapillaries) and remained nearly constant in a wide range of GO coverage (Fig. 7A), indicating that water experienced an ultrafast permeation through the nanocapillaries within GOLM, independent of their length. Differences in water flux among the three feed solutions at a fixed thickness were attributed to the different degrees of ion blockage, while the general decreased water flux compared to bare microfilter could be attributed to the encountering of a permeating energy barrier through the solution/membrane interphase. By contrast, salt flux gradually decreased with the increase of GOLM thickness (Fig. 7B), presumably due to the more effective anchoring and capture of ions from the prolonged ion–GO interactions. As shown in Fig. 7C, nominal rejection increased with GOLM thickness due to the invariable water flux and decreased salt flux. Therefore, with thick GOLM in diffusion, excellent water/ion selectivity could be achieved by taking full advantage of ion–water–GO interactions for promising water desalination. As indicated in Fig. 7C, for GOLM bearing the same thickness as that in pressurized filtration, rejection of $K_3Fe(CN)_6$ in diffusion was comparable to that in pressurized filtration, while those of K_2SO_4 and KCl were significantly higher. This indicates that based on the steric hindrance of sp^2 nanocapillaries, excellent desalination performance could be achieved in both processes to remove large molecules and ions. However, during the removal of small hydrated ions, the applied pressure seriously weakened the water/ion selectivity and degraded the desalination performance.

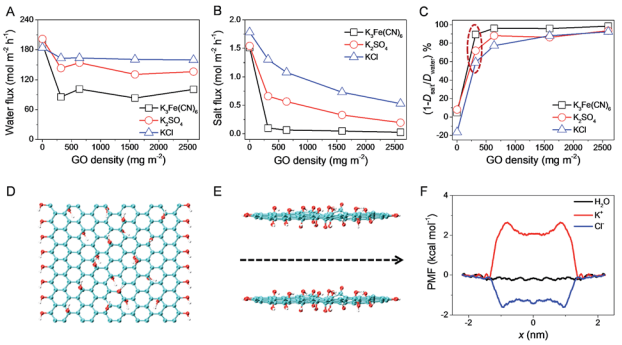

Fig. 7 Concentration gradient-driven water and salt diffusions through GOLM on a microfilter with increased GO coverage density. (A) Water fluxes, (B) salt fluxes and (C) nominal rejections. Feed concentration of salts: 0.1 M; feed concentration of D_2O: 30 wt%. (D and E) Atomic structures of GO sheets that defined a finite-length channel for ion and water diffusions in SMD simulations. (F) Free energy profiles for water and ion (K^+ and Cl^-) transport across the channel obtained from SMD simulations.

Steered molecular dynamics simulations

To gain more insight into the different transport mechanisms between water molecules and ions travelling into and out of GO nanochannels, steered molecular dynamics (SMD) simulations were performed.[20] The results illustrated in Fig. 7D and E show that the diffusion of species across GOLM was selective considering the end effects where the species needed to enter or exit the interlayer gallery between GO sheets. A substantial free energy barrier was characterized for ions such as K^+ and Cl^-, which, however, was negligible for water molecules (Fig. 7F). The results from the simulations were in excellent agreement with those from experiments (Fig. 7A and B).

Conclusions

In summary, the long-overlooked reason behind the controversy in water desalination with GOLM has been unveiled *via* combined experimental studies and MD simulations. Intrinsic high water/ion selectivity was achieved in concentration gradient-driven diffusion with great potential in water desalination, while the salt rejection of GOLM was poor in pressurized filtration. This aligned well with the reported controversial results that poor salt rejections were generally obtained with GOLM in reverse osmosis,[11–14,16] whereas the ion exclusions were excellent in forward osmosis[18] and diffusion.[19] This discrepancy was found to originate from the strong correlation of water/ion selectivity with the applied pressure and GO interlayer channel

length. The applied pressure weakened water–ion interactions confined in GO nanochannels and further reduced their selectivity, while the length of nanochannels regulated the selectivity among various salts and dominated the through-channel transport processes of water and ions. This study provides a fundamental understanding on the in-depth mechanism of water desalination with GOLMs, which is crucial to assist the future development of GOLMs in this challenging area and can be extended to other well-designed filtration and separation applications. Considering the negative role of applied pressure in the intrinsic high water/ion selectivity of GOLMs and the unique transport mechanisms of water and ions through GOLMs, forward osmosis desalination with thick GOLMs should be a promising developing direction in the future.

Acknowledgements

This work was supported by the National Natural Science Foundation of China (51372133), Tsinghua National Laboratory for Information Science and Technology (TNList) Cross-discipline Foundation and the World Premier International Center Initiative (WPI) on Materials Nanoarchitectonics, MEXT, Japan. Support from JSPS KAKENHI grants (15H03534 and 15K13296) is also acknowledged.

Notes and references

1 R. R. Nair, H. A. Wu, P. N. Jayaram, I. V. Grigorieva and A. K. Geim, *Science*, 2012, **335**, 442–444.
2 D. W. Boukhvalov, M. I. Katsnelson and Y. W. Son, *Nano Lett.*, 2013, **13**, 3930–3935.
3 R. K. Joshi, P. Carbone, F. C. Wang, V. G. Kravets, Y. Su, I. V. Grigorieva, H. A. Wu, A. K. Geim and R. R. Nair, *Science*, 2014, **343**, 752–754.
4 B. Mi, *Science*, 2014, **343**, 740–742.
5 P. Sun, M. Zhu, K. Wang, M. Zhong, J. Wei, D. Wu, Z. Xu and H. Zhu, *ACS Nano*, 2013, **7**, 428–437.
6 P. Sun, F. Zheng, M. Zhu, Z. Song, K. Wang, M. Zhong, D. Wu, R. B. Little, Z. Xu and H. Zhu, *ACS Nano*, 2014, **8**, 850–859.
7 K. Huang, G. Liu, Y. Lou, Z. Dong, J. Shen and W. Jin, *Angew. Chem., Int. Ed.*, 2014, **53**, 1–5.
8 L. Huang, Y. Li, Q. Zhou, W. Yuan and G. Shi, *Adv. Mater.*, 2015, **27**, 3797–3802.
9 G. Liu, W. Jin and N. Xu, *Chem. Soc. Rev.*, 2015, **44**, 5016–5030.
10 P. Sun, K. Wang and H. Zhu, *Adv. Mater.*, 2016, **28**, 2287–2310.
11 Y. Han, Z. Xu and C. Gao, *Adv. Funct. Mater.*, 2013, **23**, 3693–3700.
12 M. Hu and B. Mi, *Environ. Sci. Technol.*, 2013, **47**, 3715–3723.
13 J. Wang, P. Zhang, B. Liang, Y. Liu, T. Xu, L. Wang, B. Cao and K. Pan, *ACS Appl. Mater. Interfaces*, 2016, **8**, 6211–6218.
14 A. Akbari, P. Sheath, S. T. Martin, D. B. Shinde, M. Shaibani, P. C. Banerjee, R. Tkacz, D. Bhattacharyya and M. Majumder, *Nat. Commun.*, 2016, **7**, 10891.
15 H. Huang, Z. Song, N. Wei, L. Shi, Y. Mao, Y. Ying, L. Sun, Z. Xu and X. Peng, *Nat. Commun.*, 2013, **4**, 2979.
16 S. J. Gao, H. Qin, P. Liu and J. Jin, *J. Mater. Chem. A*, 2015, **3**, 6649–6654.
17 Y. Han, Y. Jiang and C. Gao, *ACS Appl. Mater. Interfaces*, 2015, **7**, 8147–8155.
18 H. Liu, H. Wang and X. Zhang, *Adv. Mater.*, 2014, **27**, 249–254.
19 P. Sun, Q. Chen, X. Li, H. Liu, K. Wang, M. Zhong, J. Wei, D. Wu, R. Ma, T. Sasaki and H. Zhu, *NPG Asia Mater.*, 2015, **7**, e162.
20 See ESI.†
21 A. V. Talyzin, T. Hausmaninger, S. You and T. Szabó, *Nanoscale*, 2014, **6**, 272–281.
22 A. Vorobiev, A. Dennison, D. Chernyshov, V. Skrypnychuk, D. Barbero and A. V. Talyzin, *Nanoscale*, 2014, **6**, 12151–12156.
23 A. Klechikov, J. Yu, D. Thomas, T. Sharifi and A. V. Talyzin, *Nanoscale*, 2015, **7**, 15374–15384.
24 K. Erickson, R. Erni, Z. Lee, N. Alem, W. Gannett and A. Zettl, *Adv. Mater.*, 2010, **22**, 4467–4472.
25 D. Pacilé, J. C. Meyer, A. Fraile Rodríguez, M. Papagno, C. Gómez-Navarro, R. S. Sundaram, M. Burghard, K. Kern, C. Carbone and U. Kaiser, *Carbon*, 2011, **49**, 966–972.
26 C. Gomez-Navarro, J. C. Meyer, R. S. Sundaram, A. Chuvilin, S. Kurasch, M. Burghard, K. Kern and U. Kaiser, *Nano Lett.*, 2010, **10**, 1144–1148.
27 H. W. Kim, H. W. Yoon, S. M. Yoon, B. M. Yoo, B. K. Ahn, Y. H. Cho, H. J. Shin, H. Yang, U. Paik, S. Kwon, J. Y. Choi and H. B. Park, *Science*, 2013, **342**, 91–95.
28 H. Li, Z. Song, X. Zhang, Y. Huang, S. Li, Y. Mao, H. J. Ploehn, Y. Bao and M. Yu, *Science*, 2013, **342**, 95–98.
29 M. R. Karim, K. Hatakeyama, T. Matsui, H. Takehira, T. Taniguchi, M. Koinuma, Y. Matsumoto, T. Akutagawa, T. Nakamura, S. Noro, T. Yamada, H. Kitagawa and S. Hayami, *J. Am. Chem. Soc.*, 2013, **135**, 8097–8100.
30 H. Huang, Y. Mao, Y. Ying, Y. Liu, L. Sun and X. Peng, *Chem. Commun.*, 2013, **49**, 5963–5965.
31 F. Fornasiero, H. G. Park, J. K. Holt, M. Stadermann, C. P. Grigoropoulos, A. Noy and O. Bakajin, *Proc. Natl. Acad. Sci. U. S. A.*, 2008, **105**, 17250–17255.

